Communications in Applied and Industrial Mathematics, DOI: 10.1685/journal.caim.000394
ISSN 2038-0909, e-394

Ghost cell boundary conditions for the Euler equations and their relationships with feedback control

Andrea Villa, Luca Barbieri, Roberto Malgesini

Transmission and Distribution Department (TTD)
Ricerca Sistema Energetico (RSE), Milano, Italy
andrea.villa@rse-web.it
luca.barbieri@rse-web.it
roberto.malgesini@rse-web.it

Communicated by Alessandro Iafrati

Abstract

Computational gasdynamics finds many applications in engineering ranging from the optimization of rocket nozzles to the study of airfoils. As a consequence, the numerical solution of the Euler equations using the finite volume method is very popular as a standard computing tool. One of the most tricky aspects in this kind of simulations is the imposition of the boundary conditions. Many approaches exist to tackle this problem and the ghost cell technique is one of the most applicable ones. In particular, this technique has already been used to enforce the wall boundary condition. In this paper the ghost cell technique is used to impose different boundary conditions such as the inflow, the pressure and the temperature ones. The merits of this technique are compared to other approaches and it is proved, under some simplifying hypotheses, that the ghost cell technique can be regarded as a local proportional feedback control. The stability and the performances of the control loop are investigated as well.

Keywords: `Boundary conditions, Euler equations, ghost cell.`

AMS Subject Classification: `65M08, 35L65`

1. Introduction.

The numerical solution of the Euler equations makes possibile to tackle many problems such as the optimization of nozzles and airfoils or, in more recent days, the full aircraft aerodynamic computing. See for instance [1–3], though there are several other works that could be mentioned in this vast field.
The solution of the Euler equations of Gasdynamics, like any other hyperbolic system of equations, has a variable number of BCs. Actually the

Received 2012 01 10. Accepted 2012 04 06. Published 2012 05 03.

number of BCs to be imposed depends on the solution and is related to the number of the characteristics that enter the domain. This creates some difficulties for the numerical approximation of the conservation laws (see [4]) because the number of BCs to be imposed is a priori unknown and since the values to be imposed are just the characteristic ones. Usually the known boundary values are the physical ones and it is necessary to translate the boundary physical states into the characteristic ones.
There are mainly two different approaches to the imposition of the BCs in the hyperbolic framework: the strong and the weak approach. The strong one is usually based on the characteristic theory: a fairly complete review can be found in [5]. We can single out three kinds of approaches, though there are many variations and combinations of these three types. The first approach is based on the direct discretization of the compatibility equations on the boundary. This method is particulary simple to implement when a structured grid is used: in [6] it is shown a reactive flow case applied to a one dimensional geometry. Then this technique has been generalized to a two dimensional geometry in [7] using a finite difference scheme. An application to the Non Reflective Boundary Conditions (NRBCs) is displayed in [8]. The compatibility-equation approach has also been extended to the finite element framework in [9].
The second strong approach we describe is the characteristic one. In this method the physical boundary conditions are translated into a proper number of characteristic invariants and these are combined with the information carried by the outgoing invariants. Finally, the complete characteristic state is translated back into the physical variables and a boundary state, consistent with the boundary conditions, is obtained. This approach has been used in [10] to implement the NRBCs.
Finally, the last strong approach we review is the extrapolation one. It is usually used in conjunction with the characteristic one, see [5]. As we have already mentioned, the strong imposition scheme aims at directly construct the solution on the boundary. On the contrary, the weak imposition scheme does not directly provide a boundary state, rather it provides a suitable boundary flux. Obviously, in many cases the boundary flux cannot be arbitrarily chosen, in fact it has to be consistent with the number of the pieces of information traveling into and out of the domain. This scheme becomes very attractive when dealing with finite volume (FV) methods [11,12] or discontinuous Galerkin (DG) ones [13]. Indeed it fits perfectly the structure of the data of these methods, it is only necessary to add a structure for the boundary elements and associate a boundary state to each boundary element.
Two main approaches are used. The first one (used in [9]) resembles very

DOI: 10.1685/journal.caim.000394

closely the strong form, since a boundary state vector is computed. However this vector, instead of being imposed as the value of the discrete solution on the boundary, is used to compute a boundary flux.
The other approach aims at directly construct a flux vector. For instance, in [14] some compatibility equations are solved and a consistent normal flux is provided. In many other cases a Riemann or an approximate Riemann solver is used to provide a proper normal flux (see [15–17]). This technique is particulary effective when dealing with the wall condition and it has been analyzed in [15] both for the wall condition and for the isothermal wall condition. In [16,17] some enhanced versions of the wall condition are developed for some curved geometry configurations.
As we have already mentioned, the ghost cell approach can be implemented very easily in the finite volume method, while other approaches such as the compatibility-equation one require a cumbersome treatment since at least another set of equations have to be solved on the boundary. Moreover the strong methods are based on the characteristic theory and they do not consider shocks. The weak approach, on the contrary, is based on the theory of the Riemann solvers which considers both shocks and rarefaction waves. From these considerations we can expect better performances from the weak method and, in this paper, we propose a numerical example to show this.
These features have convinced us that this boundary imposition scheme deserves a more appropriate analysis. In this work we prove, under some simplification hypotheses, that the ghost cell technique is, in fact, a local proportional feedback control with a noise contribution. The noise is due to the interaction between a boundary cell and the set of its neighboring internal cells. We analyze, case by case, the stability of the control loop disregarding the noise contribution. In other words, we want to guarantee that the autonomous control loop is stable. Some different ghost cell boundary imposition schemes are analyzed such as the wall, the inflow, the temperature and the pressure ones. Some numerical tests are also included to check the behavior of the different BCs.
Let us briefly present the structure of this work. In Section 2 we introduce the three dimensional Euler equations of Gasdynamics together with the thermodynamic and fluid-dynamic variables. In Section 3 we introduce the discrete setting, the mesh, the numerical flux and the finite volume scheme. In 4 we show that the ghost cell method can be regarded as a nonlinear feedback control. In Section 5 we analyze, one by one, all the external states we have proposed and the theoretical results are sustained by some numerical experiments that are shown in Section 6. A brief comparison with the strong approach is also included.

2. Euler equations.

Let us introduce the Euler equations of Gasdynamics:

$$\frac{\partial V}{\partial t} + \vec{\nabla} \cdot \vec{f} = 0 \text{ on } \Omega \times (0, \vartheta_F], \quad V = \mathcal{V} \text{ at } t = 0, \tag{1}$$

where Ω is an open subset of $\mathbb{R}^3$, ϑ_F is the final simulation time, $t \in (0, \vartheta_F]$ is the time variable, $\vec{X} \in \Omega$ is the position vector, $V(t, \vec{X})$ is the vector of the physical values, $\vec{f}$ is the flux vector, and $\mathcal{V}$ is the initial condition. We also refer to $V : \Omega \to \mathbb{R}^5$ as the exact solution. In three dimensions V has five components: the density, three momentum components and the total energy. Equation (1) is usually complemented by a set of inflow BCs that are going to be analyzed soon. Moreover

$$V = \left[\rho, \vec{m}, E^t\right], \quad \vec{f}(V) = \left[\vec{m}, \frac{\vec{m} \otimes \vec{m}}{\rho} + P\bar{\bar{I}}, (E^t + P)\frac{\vec{m}}{\rho}\right], \tag{2}$$

where ρ is the density, $\vec{m}$ is the momentum density, E^t is the total energy for unit volume, $\bar{\bar{I}}$ is the identity tensor and P is the thermodynamic pressure. Furthermore $E^t = \rho e^t$ where $e^t = e + e^k$ is the total energy for unit mass, e is the internal energy for unit mass, $e^k = |\vec{u}|^2/2$ is the kinetic energy for unit mass and $\vec{u} = \vec{m}/\rho$ is the velocity vector. We choose a polytropic ideal gas, therefore: $P = \rho RT$, $e = cvT$ and $c = \sqrt{\gamma RT}$ where $R = cp - cv$ is the thermodynamic constant of the gas, cv is the specific heat at constant volume, cp is the specific heat at constant pressure, $\gamma = cp/cv$ is the ratio of the specific heats, c is the speed of sound and T is the temperature. Moreover we also define the enthalpy $h = cpT$ and the total enthalpy $h^t = h + e^k$. Finally, for a generic vector $\vec{Y}$ we denote with Y_x, Y_y, Y_z its cartesian orthogonal components. We also use the notation Y_i, $i = 1, 2, 3$ to denote the components of $\vec{Y}$. The Euler equations of Gasdynamics form a strictly hyperbolic system since the matrix

$$A(\vec{n}) = \frac{\partial \vec{f}}{\partial V} \cdot \vec{n} \tag{3}$$

is diagonalizable for every unit vector $\vec{n}$. Therefore there are two matrices L and $R = L^{-1}$ such that $D = LAR$, where D is a diagonal matrix, R is the right eigenvector matrix and L is the left eigenvector matrix. The diagonal components of D are the eigenvalues λ_i, $i = 1, \ldots, 5$, of A i.e. $u_n - c$, u_n, $u_n + c$, u_n and u_n where $u_n = \vec{u} \cdot \vec{n}$. The explicit entries of the eigenvalues L_i, with $i = 1, \ldots, 5$ can be found in [18] .
We can now complement problem (1) with a set of BCs. On a subset of the boundary Γ of the domain Ω we consider the non penetration condition,

DOI: 10.1685/journal.caim.000394

the imposed pressure condition, the inflow condition and the imposed temperature condition. In other words, we demand that the solution satisfies

$$q_i(V) = q_i^E, \quad i = 1, \dots, N_v \tag{4}$$

on the boundary, where q_i^E is the expected value on the boundary and N_v is the number of boundary conditions being imposed. Then we set

- for the wall condition: $N_v = 1$, $q_1^E = 0$ and $q_1 = (\vec{m} \cdot \vec{n})/\rho$;
- for the pressure condition: $N_v = 1$, $q_1^E = P^E$, where P^E is a given pressure and $q_1(V) = (\gamma - 1)\left(E^t - |\vec{m}|^2/(2\rho)\right)$;
- for the inflow condition: $N_v = 3$, $q_1^E = u_x^E$, $q_2^E = u_y^E$, $q_3^E = u_z^E$, where $\vec{u}^E = [u_x^E, u_y^E, u_z^E]$ is a given velocity vector and $q_1(V) = m_x/\rho$, $q_2(V) = m_y/\rho$, $q_3(V) = m_z/\rho$;
- for the temperature case: $N_v = 1$, $q_1(V) = \left(E^t/\rho - |\vec{m}|^2/(2\rho)\right)/cv$, $q_1^E = T^E$, where T^E is a given temperature.

3. Discrete method.

Let $\mathcal{T}_\Delta$ be a three dimensional symplectic grid, see Figure 1 (for the sake of clarity a 2d example is shown), with N_e elements τ_k, $k = 1, \dots, N_e$, moreover let Δ be their characteristic length. The boundary of Ω is approximated by N_b boundary elements Γ_r, $r = 1, \dots, N_b$ and let r_k be the index of the boundary element such that $\Gamma_{r_k} \bigcap \tau_k$ is a face of τ_k, see Figure 1(a). Let us denote by k_j, $j = 1, \dots, 4$ the set of indices of the cells (i.e. elements) τ_{k_j} surrounding τ_k and let us denote by $\vec{n}_k^j$ the normal to l_k^j which is the j-th face of τ_k, see Figure 1(b). Finally let $\vec{n}_r$ be the normal to Γ_r, in particular $\vec{n}_{r_k}$ is the outward normal of the r_k-th boundary element.

We denote by Ext the set of the indices k such that τ_k is a boundary cell, i.e. $Ext = \{k \in [1, N_e] : \tau_k \cap \partial\Omega = \Gamma_{r_k}\}$. The complementary set, i.e the set of the interior cells, is denoted by Int. Moreover let

$$F(V_l, V_r, \vec{n}) = \frac{1}{2}\left(\vec{f}(V_l) + \vec{f}(V_r)\right) \cdot \vec{n} - \frac{1}{2}|A(V_I(V_l, V_r), \vec{n})|(V_r - V_l) \tag{5}$$

be the Roe flux (see [12]) where V_r, V_l are the right and left states, $|A| = R|D|L$, being $|D|$ the diagonal matrix of the absolute values of the eigenvalues, and $V_I(V_l, V_r)$ is a suitable interface state defined by the Roe's average, see [12]. The Roe flux satisfies the following properties for every unit vector $\vec{n}$:

$$\begin{cases} A(V_I, \vec{n})(V_l - V_r) = (\vec{f}(V_l) - \vec{f}(V_r)) \cdot \vec{n}, \\ A(V_I, \vec{n}) \text{ is diagonalizable with real eigenvalues,} \\ A(\overline{V}, \vec{n}) \to \frac{\partial \vec{f}(\overline{V})}{\partial V} \cdot \vec{n} \text{ smoothly as } V_l, V_r \to \overline{V}. \end{cases} \tag{6}$$

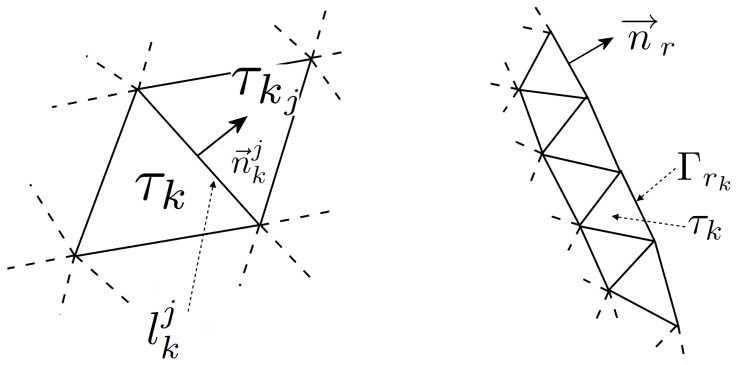

(a) (b)

Figure 1. An outline of a two dimensional representation of the mesh interior (a), and a two dimensional representation of the boundary mesh (b).

In order to introduce the discrete scheme we consider a partition of the interval $[0, \vartheta_F]$ i.e. $[t^0, t^1, \ldots, t^p, \ldots, t^{N_t}]$ where t^p is the p-th time step, N_t is the total number of the time steps and $\Delta t^p = t^{p+1} - t^p$ is the time increment. We consider the following finite volume scheme discretized with the Euler time-stepping method:

$$
\begin{cases}
V_k^{p+1} = V_k^p - \sum_{j=1}^4 \frac{|l_k^j|\Delta t^p}{|\tau_k|} F(V_k^p, V_{k_j}^p, \vec{n}_k^j) \quad k \in Int \\
V_k^{p+1} = V_k^p - \sum_{j=1}^3 \frac{|l_k^j|\Delta t^p}{|\tau_k|} F(V_k^p, V_{k_j}^p, \vec{n}_k^j) - \\
\frac{|\Gamma_{r_k}|\Delta t^p}{|\tau_k|} F(V_k^p, G(V_k^p, \psi_1, \ldots, \psi_{N_p}), \vec{n}_{r_k}) \quad k \in Ext,
\end{cases} \tag{7}
$$

where G is a proper ghost state function for the imposition of the BCs, ψ_i, with $i = 1, \ldots, N_p$, are some parameters that are specified differently for the various BCs, N_p is the number of those parameters and V_k^p is the discrete mean value of the solution in the cell τ_k at time t^p. For the sake of simplicity, in equation (7) we have assumed that the local boundary face is the fourth. In fact, in three dimensions each internal tetrahedron has four neighboring elements and each boundary tetrahedron has three.

Remark 3.1. The choice of a finite volume scheme with a Roe numerical flux simplifies the analysis of the method and the notation. However our results can be extended to other numerical fluxes satisfying (6) and to other numerical schemes such as [19]. Moreover in Section 6 we will show that, from an experimental point of view, our theory works also for other methods such as the Discontinuous Galerkin one [13].

DOI: 10.1685/journal.caim.000394

For each physical BC we use a different function G, for instance, for the wall condition, we have considered the following two functions:

(8)
$$G(V_k^p) = \left[\rho_k^p, -\vec{m}_k^p, E_k^{t,p}\right],\ G(V_k^p, \vec{n}_{r_k}) = \left[\rho_k^p, \vec{m}_k^p - 2(\vec{m}_k^p \cdot \vec{n}_{r_k})\vec{n}_{r_k}, E_k^{t,p}\right].$$

For the imposed pressure case we use

$$G(V_k^p, P^E) = \left[\rho_k^p, \vec{m}_k^p, \frac{P^E}{\gamma - 1} + \frac{|\vec{m}_k^p|^2}{2\rho_k^p}\right], \tag{9}$$

and for the inflow case we use

$$G(V_k^p, u_x^E, u_y^E, u_z^E) = \left[\rho_k^p, \rho_k^p \vec{u}^E, E_k^{t,p}\right]. \tag{10}$$

Finally, for the imposed temperature case we consider

$$G(V_k^p, T^E) = \left[\rho_k^p, \vec{m}_k^p, \rho_k^p \left(cvT^E + \frac{1}{2}\frac{|\vec{m}_k^p|^2}{\rho_k^p}\right)\right]. \tag{11}$$

4. A simplified problem.

We now consider the second equation of (7). If the cfl number is small and if the reference values q_i^E, with $i = 1, \ldots, N_v$, are constant, or weakly varying in time, it can be greatly simplified, so that we can show that the ghost cell technique is in fact a nonlinear proportional control loop.

Theorem 4.1. *If* $\frac{\Delta t^p |\Gamma_{r_k}|}{|\tau_k|} \ll 1$, $\forall k \in Ext$, $\forall p$ *and if* q_i^E *is constant in time, then*

$$q_i(V_k^{p+1}) - q_i^E = q_i(V_k^p) - q_i^E - \frac{|\Gamma_{r_k}|\Delta t^p}{|\tau_k|} \sum_{l \in In} \beta_l \lambda_l d_l + \phi_i, \tag{12}$$

where $\phi_i = \left(\frac{\partial q_i}{\partial V_k}(V_k^p)\right)\Phi$, $\frac{\partial q_i}{\partial V_k}(V_k^p)$ is the gradient of q_i with respect to the conservative variables evaluated in V_k^p and

$$\Phi = -\sum_{j=1}^{3} \frac{\Delta t^p |l_k^j|}{|\tau_k|} \left(\frac{1}{2}(A_I^j - |A_I^j|)(V_{k_j}^p - V_k^p)\right), \tag{13}$$

where $A_I^j = A(V_I(V_k^p, V_{k_j}^p), \vec{n}_k^j)$, with $j = 1, 2, 3$. Moreover

$$\beta_l = \frac{\partial q_i}{\partial V_k}(V_k^p) R_l, \tag{14}$$

$In = \{i \in [1,5] : \lambda_i < 0\}$ and

$$d_l = L_l(G(V_k^p, \psi_1, \ldots, \psi_{N_p}) - V_k^p), \tag{15}$$

where R_l and L_l are here the right and left eigenvalues of $A_I = A(V_I(V_k^p, G(V_k^p, \psi_1, \ldots, \psi_{N_p})), \vec{n}_{r_k})$. Equation (12) states that the difference between the expected boundary value q_i^E and the computed one $q_i(V_k^p)$ at the next step $p+1$ equals the one at the current step p plus a feedback contribution and an error contribution. A scheme of the feedback control is depicted in Figure 2. Now we prove the result (12)

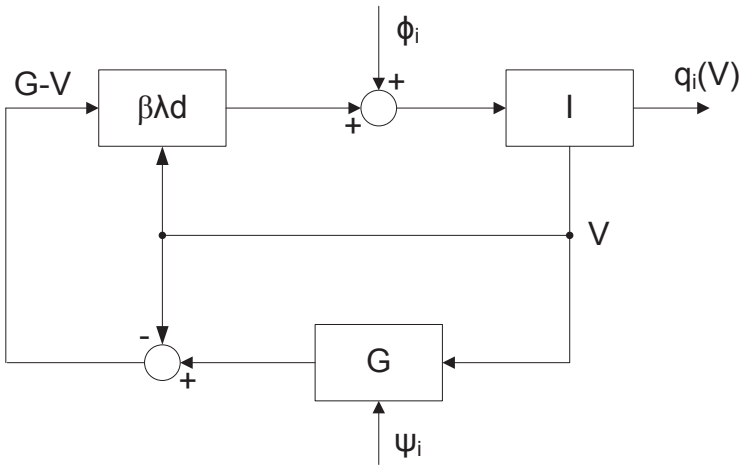

Figure 2. The control system structure. The I block is the discrete time integrator that advances the state V in time. Then the G state is computed and the difference $G - V$ is combined computing the d_l, λ_l and β_l quantities to get the updated control signal.

Proof. First we consider the second equation of (7) and adding

$$\frac{\Delta t^p |\Gamma_{r_k}|}{|\tau_k|} F(V_k^p, V_k^p, \vec{n}_{r_k}) + \sum_{j=1}^{3} \frac{\Delta t^p |l_k^j|}{|\tau_k|} F(V_k^p, V_k^p, \vec{n}_k^j) = 0 \tag{16}$$

we get

$$\begin{aligned} V_k^{p+1} - V_k^p + \sum_{j=1}^{3} \frac{\Delta t^p |l_k^j|}{|\tau_k|} \left(F(V_k^p, V_{k_j}^p, \vec{n}_k^j) - F(V_k^p, V_k^p, \vec{n}_k^j) \right) \\ + \frac{\Delta t^p |\Gamma_{r_k}|}{|\tau_k|} \left(F(V_k^p, G(V_k^p, \psi_1, \ldots, \psi_{N_p}), \vec{n}_{r_k}) - F(V_k^p, V_k^p, \vec{n}_{r_k}) \right) = 0, \end{aligned} \tag{17}$$

DOI: 10.1685/journal.caim.000394

then, using the numerical flux definition (5), we have

(18)
$$V_k^{p+1} - V_k^p + \sum_{j=1}^{3} \frac{\Delta t^p |l_k^j|}{|\tau_k|} \left(\frac{1}{2} \left(\vec{f}(V_{k_j}^p) - \vec{f}(V_k^p) \right) \cdot \vec{n}_k^j - \frac{1}{2} |A_I^j| (V_{k_j}^p - V_k^p) \right) + \frac{\Delta t^p |\Gamma_{r_k}|}{|\tau_k|} \left(\frac{1}{2} \left(\vec{f}(G(V_k^p, \psi_1, \ldots, \psi_{N_p})) - \vec{f}(V_k^p) \right) \cdot \vec{n}_{r_k} - \frac{1}{2} |A_I| (G(V_k^p, \psi_1, \ldots, \psi_{N_p}) - V_k^p) \right) = 0,$$

and, using the numerical flux consistency relations (6), we get

(19)
$$V_k^{p+1} - V_k^p + \sum_{j=1}^{3} \frac{\Delta t^p |l_k^j|}{|\tau_k|} \left(\frac{1}{2} (A_I^j - |A_I^j|)(V_{k_j}^p - V_k^p) \right) + \frac{\Delta t^p |\Gamma_{r_k}|}{|\tau_k|} \left(\frac{1}{2} (A_I - |A_I|)(G(V_k^p, \psi_1, \ldots, \psi_{N_p}) - V_k^p) \right) = 0.$$

Then, using (13) and the eigenvalue decomposition of A_I, we obtain

(20)
$$V_k^{p+1} = V_k^{\Delta,p} - \frac{\Delta t^p |\Gamma_{r_k}|}{|\tau_k|} \left(R \frac{|D| - D}{2} L \right) (G(V_k^p, \psi_1, \ldots, \psi_{N_p}) - V_k^p) + \Phi.$$

The matrix $(|D| - D)/2$ is a diagonal matrix with the following entries:

(21)
$$\frac{|D_{ii}| - D_{ii}}{2} = \begin{cases} 0 & \text{if } \lambda_i \geq 0, \\ -\lambda_i & \text{if } \lambda_i < 0. \end{cases}$$

Then, since on the boundary we expect that (4) is satisfied, we apply $q_i(\cdot)$ to (20) getting

(22)
$$q_i(V_k^{p+1}) = q_i \left(V_k^p - \frac{|\Gamma_{r_k}| \Delta t^p}{|\tau_k|} \frac{1}{2} (A_I - |A_I|)(G - V_k^p) + \Phi \right),$$

where $i = 1, \ldots, N_v$. This last equation provides a fully nonlinear dynamic system which, in its general form, is almost untractable. Therefore, as we have supposed that the cfl number is small, we linearize it with respect to Δt^p and we obtain:

(23)
$$q_i(V_k^{p+1}) = q_i(V_k^p) - \frac{|\Gamma_{r_k}| \Delta t^p}{|\tau_k|} \left(\frac{\partial q_i}{\partial V_k}(V_k^p) \right) R \frac{D - |D|}{2} L(G - V_k^p) + \phi_i + O(\Delta t^2).$$

Equation (23) can also be written, using (14), (15) and (21), as:

$$q_i(V_k^{p+1}) = q_i(V_k^p) - \frac{|\Gamma_{r_k}|\Delta t^p}{|\tau_k|} \sum_{l \in In} \beta_l \lambda_l d_l + \phi_i, \tag{24}$$

where we have truncated the second order terms. Then, if we consider a nearly time-constant BC, we can subtract q_i^E from both sides of (24) obtaining the thesis. □

We still have a nonlinear dynamic system though equation (12) has a relatively simple structure that can be treated using the control theory, see for instance [20].

5. Consistency and stability analysis.

For each BC we analyze whether the control loop is active and stable. In general the control loop becomes inactive if there are no characteristics that enter the domain. The stability of the control loop does not imply the convergence of the whole scheme, however in the result section we show that the weak method has good performances and the failure reasons can be explained by the theory we have developed.
In the remainder of this Section, since we refer to a generical cell $k \in Ext$ and to the related boundary element Γ_{r_k}, we'll drop, for the sake of simplicity, the indices k and r whereas we retain the time-step index p. Finally, since we are interested in the stability of the autonomous loop control, we neglect the contribution of ϕ_i in (24)

5.1. *Non penetration.*

For the first of the boundary states in (8) we have, using the Roe's average state definition, see [12], that $\vec{u}_I^p = 0$ therefore $In = \{1\}$ and the control loop is always active. From (15) we get

$$d_1 = L_1^T \left(\left[\rho^p, -\vec{m}^p, E^{t,p} \right] - \left[\rho^p, \vec{m}^p, E^{t,p} \right] \right), \tag{25}$$

and using the definition of L_1, see [18], we have

$$d_1 = \frac{(1-\gamma)\vec{u}_I^p - c_I^p \vec{n}}{(c_I^p)^2} \cdot (-2\vec{m}^p) = \frac{2\rho^p u_n^p}{c_I^p}. \tag{26}$$

Moreover from (14) we compute $\beta_1 = -(u_n^p + c_I^p)/\rho^p$ and then, substituting this and (26) into (12), we get

$$u_n^{p+1} = u_n^p - 2\frac{|\Gamma|\Delta t^p (u_n^p + c_I^p)}{|\tau|} u_n^p. \tag{27}$$

DOI: 10.1685/journal.caim.000394

The previous equation is stable if $|1-2(|\Gamma|\Delta t^p/|\tau|)(u_n^p+c_I^p)|<1$ and this reduces to $(|\Gamma|\Delta t^p/|\tau|)(u_n^p+c_I^p)<1$, and $u_n^p>-c_I^p$. The first condition is a standard cfl stability condition (see [12]) while the second one requires that the normal speed is bounded from below by c_I^p which is the speed of sound associated with the Roe's interface state.
Elaborating these two bounds, and since $u_n^E=0$, we get that $-c_I^p<u_n^p-u_n^E<(|\tau|/|\Gamma|\Delta t^p)-c_I^p$. In other words, if the normal speed (u_n^p) differs too much from the desired value ($u_n^E=0$), the system will be no longer stable and, according to the linear analysis, it will blow up. Similar results can be found for the second wall imposition scheme.

5.2. *Inflow.*

The stability analysis of this BC is somehow more difficult, in fact by now we have analyzed a boundary condition that involves only a time-difference equation. However the inflow condition requires the solution of three coupled difference equations. This makes the analysis much more difficult and some simplifying hypotheses have to be added. In particular we study this BC only in some relevant cases.
This boundary condition becomes active if there is at least one characteristic entering the domain. However, in that case only one piece of information (the normal speed) is imposed. The control on all the components of the speed vector becomes available when the following condition is satisfied: $u_n^p<-u_n^E/2$ with u_n^E negative.
We compute the d_l vectors:

$$d_1=\rho\left(\frac{1-\gamma}{2(c_I^p)^2}\vec{u}_I^p-\frac{\vec{n}}{2c_I^p}\right)\cdot\left(\vec{u}^E-\vec{u}^p\right),\ d_2=\rho\frac{\gamma-1}{(c_I^p)^2}\vec{u}_I^p\cdot\left(\vec{u}^E-\vec{u}^p\right),$$

$$d_3=\rho\left(\frac{1-\gamma}{2(c_I^p)^2}\vec{u}_I^p+\frac{\vec{n}}{2c_I^p}\right)\cdot\left(\vec{u}^E-\vec{u}^p\right),$$

$$d_4=\rho\left[\left(u_x^E-u_x^p\right)n_y+\frac{n_y^2-1}{n_x}\left(u_y^E-u_y^p\right)+\frac{n_yn_z}{n_x}\left(u_z^E-u_z^p\right)\right],$$

$$d_5=\rho\left[-n_z\left(u_x^E-u_x^p\right)-\frac{n_yn_z}{n_x}\left(u_y^E-u_y^p\right)+\frac{1-n_z^2}{n_x}\left(u_z^E-u_z^p\right)\right],$$

(28)

and the β_l vectors:

$$\beta_1=\frac{1}{\rho^p}(u_i^E-u_{I,i}^p-c_I^pn_i),\ \beta_2=\frac{1}{\rho^p}(u_i^E-u_{I,i}^p),$$

$$\beta_3=\frac{1}{\rho^p}(u_i^E-u_{I,i}^p+c_I^pn_i),\ \beta_4=\begin{cases}-\frac{1}{\rho^p}\text{ if }i=2\\0\text{ otherwise}\end{cases},\ \beta_5=\begin{cases}\frac{1}{\rho^p}\text{ if }i=3\\0\text{ otherwise}\end{cases},$$

(29)

where $i = 1, 2, 3$ and u_i^E, $u_{I,i}^p$, n_i are the components of the $\vec{u}^E$, $\vec{u}_I^p$ and $\vec{n}$ vectors. We suppose $\vec{u}_I^p \approx \vec{u}^E$ i.e. the interface speed close to the desired one. Under these hypotheses the values in equations (29) can be simplified:

(30)
$$\beta_1 \approx -\frac{c_I^p n_i}{\rho^p},\ \beta_2 \approx 0,\ \beta_3 \approx \frac{c_I^p n_i}{\rho^p},\ \beta_4 = \begin{cases} -\frac{1}{\rho^p} \text{ if } i = 2; \\ 0 \text{ otherwise} \end{cases},\ \beta_5 = \begin{cases} \frac{1}{\rho^p} \text{ if } i = 3; \\ 0 \text{ otherwise} \end{cases}.$$

Moreover we choose $\vec{n} = \{1, 0, 0\}$; this is not limitative since we can always choose a local reference system such that the normal vector is aligned with the first coordinate. We are now ready to study the system in some relevant conditions:

- slow speed: $|\vec{u}^E| \ll c_I^p$, $|\vec{u}_n^E| \ll c_I^p$, $\vec{u}_n^E < 0$. In this case the approximated eigenvalues are:

  (31) $$\lambda_1 \approx -c_I^p, \quad \lambda_2 = \lambda_4 = \lambda_5 \approx \vec{u}_n^E, \quad \lambda_3 \approx c_I^p,$$

  while the approximation of the d_l vectors is:

  (32) $$d_1 \approx -\rho^p \frac{\vec{n}}{2c_I^p} \cdot (\vec{u}^E - \vec{u}^p),\ d_2 \approx 0,\ d_3 \approx \rho^p \frac{\vec{n}}{2c_I^p} \cdot (\vec{u}^E - \vec{u}^p),$$
  $$d_4 \approx -\rho^p (u_y^E - u_y^p),\ d_5 \approx -\rho^p (u_z^E - u_z^p).$$

  Therefore, substituting (30), (31) and (32) into (12), we obtain the following approximated dynamical system:

  (33) $$\begin{bmatrix} u_x^{p+1} - u_x^E \\ u_y^{p+1} - u_y^E \\ u_z^{p+1} - u_z^E \end{bmatrix} = \begin{bmatrix} \mu_1 & 0 & 0 \\ 0 & \mu_2 & 0 \\ 0 & 0 & \mu_3 \end{bmatrix} \begin{bmatrix} u_x^p - u_x^E \\ u_y^p - u_y^E \\ u_z^p - u_z^E \end{bmatrix},$$

  where $\mu_1 = 1 - (|\Gamma|\Delta t^p c_I^p)/(2|\tau|)$, $\mu_2 = 1 + (|\Gamma|\Delta t^p u_n^E)/|\tau|$ and $\mu_3 = 1 + (|\Gamma|\Delta t^p u_n^E)/|\tau|$. Since the matrix is diagonal we have only to check that the entries belong to the interval $(-1, 1)$ and this leads to the standard cfl condition.
- sonic transition with $In = \{1, 2, 4, 5\}$: $|\vec{u}_n^E| \approx c_I^p$, $u_n^E < 0$. In this case the approximation of the eigenvalues is: $\lambda_1 \approx -2c_I^p$, $\lambda_2 = \lambda_4 = \lambda_5 \approx -c_I^p$ and $\lambda_3 \approx 0$. Consequently the dynamical system becomes

  (34) $$\begin{bmatrix} u_x^{p+1} - u_x^E \\ u_y^{p+1} - u_y^E \\ u_z^{p+1} - u_z^E \end{bmatrix} = \begin{bmatrix} \mu_1 & (\gamma - 1)u_y^E & (\gamma - 1)u_z^E \\ 0 & \mu_2 & 0 \\ 0 & 0 & \mu_3 \end{bmatrix} \begin{bmatrix} u_x^p - u_x^E \\ u_y^p - u_y^E \\ u_z^p - u_z^E \end{bmatrix},$$

DOI: 10.1685/journal.caim.000394

where $\mu_1 = 1-(|\Gamma|\Delta t^p/|\tau|)((\gamma-1)u_x^E+c_I^p)$, $\mu_2 = 1+(|\Gamma|\Delta t^p u_n^E/|\tau|)$ and $\mu_3 = 1+(|\Gamma|\Delta t^p u_n^E/|\tau|)$. Since we have a scale matrix, all the eigenvalues of the linearized dynamical system are on the diagonal. Then, since by hypothesis $u_n^E = u_x^E = -c_I^p$, we get that the stability condition is satisfied provided that the cfl condition is satisfied.

- sonic transition with $In = \{1,2,4,5\}$: $|\vec{u}_n^E| \approx c_I^p$, $u_n^E < 0$. It is the same as above, since $\lambda_3 \approx 0$.

- supersonic inflow: $|\vec{u}_n^E| \gg c_I^p$, $u_n^E < 0$. In this case the dynamical system is

$$\begin{bmatrix} u_x^{p+1} \\ u_y^{p+1} \\ u_z^{p+1} \end{bmatrix} = \begin{bmatrix} \mu & 0 & 0 \\ 0 & \mu & 0 \\ 0 & 0 & \mu \end{bmatrix} \begin{bmatrix} u_x^p - u_x^E \\ u_y^p - u_y^E \\ u_z^p - u_z^E \end{bmatrix}, \tag{35}$$

where $\mu = 1+(|\Gamma|\Delta t^p/|\tau|)u_n^E$. And this, if the cfl condition is satisfied, is stable.

5.3. *Imposed pressure.*

This BC becomes active if: $(M_{I,n}^p)^2 = (u_{I,n}^p/c_I^p)^2 < 1$. This is equivalent to:

$$\frac{P^p + P^E}{2} > \rho\left((u_n^p)^2 + (\gamma-1)^2 e^{k,p}\right). \tag{36}$$

Let us now discuss the stability. We have:

$$d_1 = \frac{P^E - P^p}{2(c_I^p)^2}, \quad d_2 = -\frac{P^E - P^p}{(c_I^p)^2}, \quad d_3 = \frac{P^E - P^p}{2(c_I^p)^2}, \quad d_4 = 0, \quad d_5 = 0, \tag{37}$$

and

$$\beta_1 = \beta_3 = \frac{\gamma-1}{2}\left(h^p + \frac{\gamma}{\gamma-1}\frac{P^E}{\rho^p}\right), \ \beta_2 = 0, \ \beta_4 = 0, \ \beta_5 = 0, \tag{38}$$

therefore, if $In = \{1\}$ or $In = \{1,2,4,5\}$, then

$$\sum_{l\in In} \beta_l \lambda_l d_l = \frac{1}{2}\frac{\beta_1}{(c_I^p)^2}(u_{I,n}^p - c_I^p)(P^E - P^p). \tag{39}$$

Using [18] and (14) we compute

$$\beta_1 = (\gamma-1)\frac{|\vec{u}^p|^2}{2} - (\gamma-1)\vec{u}^p\cdot\left(\vec{u}_I^p - c_I\vec{n}\right) + (\gamma-1)\left(h_I^{t,p} - c_I^p(\vec{u}_I^p\cdot\vec{n})\right). \tag{40}$$

Then, using (9) and the Roe's interface state definition, see [12], we get: $\rho_I = \rho^p$, $\vec{u}_I = \vec{u}^p$. Therefore we get $\beta_1 = (\gamma - 1)h_I^p \equiv (c_I^p)^2$ and equation (39) reduces to

$$\sum_{l \in In} \beta_l \lambda_l d_l = \frac{1}{2}(u_{I,n}^p - c_I^p)(P^E - P^p), \tag{41}$$

and from (12), neglecting the error ϕ_i, we obtain

$$P^{p+1} - P^E = \left(1 + \frac{|\Gamma|\Delta t^p}{|\tau|}\frac{1}{2}(u_{I,n}^p - c_I^p)\right)(P^p - P^E). \tag{42}$$

Then, since here we have considered a subsonic inflow case, $u_{I,n}^p - c_I^p < 0$, we get that the loop is stable if $(|\Gamma|\Delta t^p/|\tau|)(u_{I,n}^p - c_I^p) > -1$ that can be regarded as a standard cfl condition. Similar results can be proven for the supersonic inflow case.

5.4. *Temperature.*

The temperature BC becomes active for

$$(u_n^p)^2 < \frac{1}{2}\left[(c^p)^2 + (\gamma - 1)\left(cvT^E - \gamma e^{k,p}\right)\right]. \tag{43}$$

The d_l vectors are:

$$d_1 = \frac{\gamma - 1}{2(c_I^p)^2}\rho^p cv(T^E - T^p),\ d_2 = \frac{1 - \gamma}{(c_I^p)^2}\rho^p cv(T^E - T^p), \tag{44}$$
$$d_3 = \frac{\gamma - 1}{2(c_I^p)^2}\rho^p cv(T^E - T^p),\ d_4 = 0,\ d_5 = 0,$$

and the β_l vectors are:

$$\beta_1 = \beta_3 = \frac{1}{\rho^p}\left(T^E + (\gamma - 2)T_I^p\right),\ \beta_2 = \frac{1}{\rho^p}\left(T^E - 2T_I^p\right),\ \beta_4 = \beta_5 = 0. \tag{45}$$

Then, if $In = \{1\}$, we have

$$\sum_{l \in In} \beta_l \lambda_l d_l = -(T^E + (\gamma - 2)T_I^p)(u_{I,n}^p - c_I^p)\frac{\gamma - 1}{2(c_I^p)^2}cv(T^p - T^E). \tag{46}$$

Using the same procedure as in the previous BCs and combining (46) with (12) we get that this BC is stable if $T^E/(3\gamma + 2) < T_I^p < T^E/(2 - \gamma)$. Then,

DOI: 10.1685/journal.caim.000394

if we consider the case $In = \{1, 2, 4, 5\}$, we get

$$\sum_{l \in In} \beta_l \lambda_l d_l = \left(-(T^E + (\gamma - 2)T_I^p)(u_{I,n}^p - c_I^p) cv \frac{\gamma - 1}{2(c_I^p)^2} + (T^E - 2T_I^p) u_{I,n}^p cv \frac{\gamma - 1}{(c_I^p)^2} \right) (T^p - T^E). \tag{47}$$

A set of conditions for the stability of (47) is:

$$0 < (T^E + (\gamma - 2)T_I^p) cv \frac{\gamma - 1}{(c_I^p)^2} < 1, \quad 0 < -(T^E - 2T_I^p) \frac{\gamma - 1}{(c_I^p)^2} cv < \frac{1}{2}. \tag{48}$$

Finally, considering the supersonic inflow condition $In = \{1, 2, 3, 4, 5\}$, we have

$$\sum_{l \in In} \beta_l \lambda_l d_l = \left(-(T^E + (\gamma - 2)T_I^p)(u_{I,n}^p - c_I^p) cv \frac{\gamma - 1}{2(c_I^p)^2} + (T^E - 2T_I^p) u_{I,n}^p \frac{\gamma - 1}{(c_I^p)^2} cv - (T^E + (\gamma - 2)T_I^p)(u_{I,n}^p + c_I^p) cv \frac{\gamma - 1}{2(c_I^p)^2} \right) (T^p - T^E). \tag{49}$$

Following the same procedure as in the previous cases we can deduce that a set of conditions for the stability is:

$$0 < (T^E + (\gamma - 2)T_I^p) cv \frac{\gamma - 1}{(c_I^p)^2} < 1, \quad 0 < (T^E - 2T_I^p) \frac{\gamma - 1}{(c_I^p)^2} cv < 1. \tag{50}$$

6. Numerical results.

6.1. *Supersonic flow in a channel.*

The purpose of this test case is to check the correct behavior of the boundary imposition scheme using a test case derived from a standard gas dynamic application. In particular we have simulated the interactions inside a channel using a supersonic flow. This test case can be directly compared to the first test case displayed in [9]. There, a strong approach based on the discretization of the compatibility equations coupled with a Taylor-Galerkin finite element method is used. The channel has a couple of solid walls on the top and on the bottom. On the bottom a 5 degrees symmetric ramp with a length of 6 units (can be thought as meters) is added. The boundary conditions are complemented by some supersonic inflow and outflow conditions on the left and on the right. The inflow conditions are: $P = 101325$ Pa, $T = 300$ K and $u = 868 m/s$. These conditions correspond to a Mach

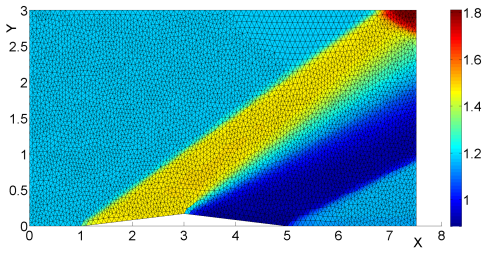

Figure 3. The density field in a channel.

number of 2.5. The ramp generates a shock wave which interferes with the solid wall on the top of the channel. Our results in Figure 3 show that the weak boundary method can obtain the same correct results displayed in [9]. However the approach used there requires the explicit solution of a partial differential equation discretized with the finite element technique and this adds complexity and computational costs. On the contrary, the weak approach requires only the solution of some Riemann problems on the boundary. Moreover the weak approach can be easily generalized to higher order methods in fact, in this case, we have used a linear discontinuous Galerkin method.

6.2. *Stability analysis.*

In this test we want to compare the behavior of the strong approach with the weak one in terms of stability. In the literature there are a few works that investigate the conditions under which the strong imposition scheme may fail, among them we have implemented some representative techniques against which we compare the performances of the weak approach. As we have already mentioned, there are many strong imposition methods, therefore we have selected a few techniques that are particulary suited to the finite volume approach. In this particular case we have used the characteristic methods described in [5], page 349, for the inflow and outflow conditions and a flux method coupled with a pressure extrapolation to impose the wall condition, see [5], page 379. We consider a rhombus-shaped airfoil contained in a box-shaped domain, see Figure 4(a). The rhombus is 0.1-thick and 0.6 long, while the containing box is 1-long and 1-high.
The gasdynamic simulation codes have been extensively used to predict the flow field past an airfoil and this test case can be regarded as a typical application of these computing tools. In this test case we have chosen a particular couple of boundary and initial conditions to show that the weak imposition scheme has better performances than the strong one. In

DOI: 10.1685/journal.caim.000394

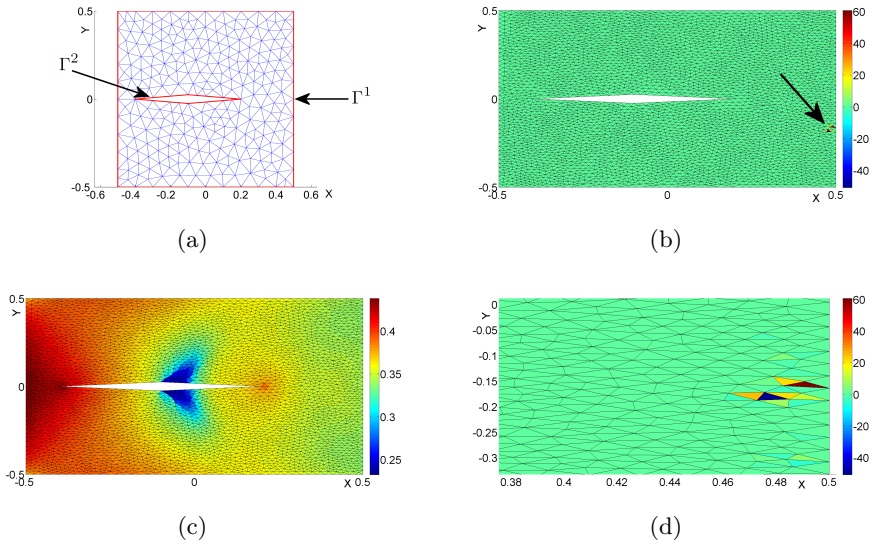

Figure 4. (a) A rhombus-shaped airfoil contained in a box-shaped domain. On Γ^1 the entire state is fixed, while on Γ^2 we apply a non penetration condition. (b) The density field using a strong boundary imposition scheme and (c) using a weak one. In (d) a detail of the failure of the strong scheme is depicted.

particular we have chosen the following initial conditions:

$$\left[0.36\ kg/m^3, [-100, 0]\ \ kg/(m^2 s), 7.5983 \cdot 10^4\ J/m^3\right]. \tag{51}$$

The boundary state we want to impose is:

$$\left[0.36\ kg/m^3, [300, 0]\ \ kg/(m^2 s), 9.0383 \cdot 10^4\ J/m^3\right]. \tag{52}$$

These conditions create a shock on the left side of the domain and a strong rarefaction wave on the right side. As we can see in Figure 4(b), the boundary imposition scheme generates, in a few steps, some instabilities in the vicinity of the boundary. Here the density reaches some negative values leading to the breakdown of the scheme. On the contrary, the weak scheme remains stable and generates an acceptable solution, see Figure 4(c).
The strong imposition scheme, as described in [5], is based on a linearization of the Euler equations on boundary. However the linearization is valid only for small variations in time of the state on the boundary. Therefore shock-waves and strong rarefactions may lead to inaccurate computations or even instabilities.

6.3. *Nozzle.*

In this test case we want to compare the strong approach with the weak one using a time dependent boundary condition. As we have already mentioned, the strong boundary imposition schemes often require a linearization of the compatibility equations on the boundary. Therefore, if the boundary condition is varying quickly enough we may expect to observe some inaccuracies on the boundary.
We have considered a planar nozzle with an inlet length of 2 units (can be thought as meters), a throat of 0.4 units and an exhaust of 3.6 units. On the inlet we impose an inflow condition with a speed of 50 m/s and a density of 1.18 kg/m^3, while on the outflow we impose an oscillating pressure $P = 50000 + 40000\sin(\pi(t/0.0040))\ Pa$, with t expressed in seconds. The results are shown in Figure 5. The two solutions are similar though there are

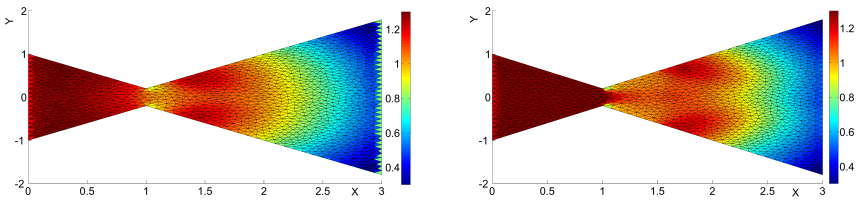

(a) (b)

Figure 5. The density field in a double-conic nozzle using a strong (a) and a weak (b) approach.

some small differences in the convergent part of the nozzle. The other most notable feature is that the weak imposition method does not produce any spurious effect on the boundary. In Figure 5(a) we can clearly see that the triangles on the outflow boundary have a density that is slightly different from the one of the neighboring triangles: this creates a clearly jagged profile on the outflow boundary. On the contrary, the weak imposition scheme has a smoother transition.
This effect is almost absent in all the simulations where the boundary conditions are constant in time while it is often present where time-varying conditions are considered. In these cases, the weak boundary conditions clearly show a better behavior.

7. Conclusions.

We have described a local criterion for predicting the performances of the BCs of strictly hyperbolic systems. The analysis has proven useful in predicting some behaviors observed in the numerical tests. Our linearized

DOI: 10.1685/journal.caim.000394

analysis has shown that the ghost cell boundary imposition scheme behaves as a non linear feedback control and some criteria have been discussed to define in which cases the feedback control is effective. With our analysis many more boundary ghost states can be easily checked. Although the verification of the stability of the control loop with a specific boundary state is highly problem-dependent, as it depends on the eigenstructure of the hyperbolic system, the extension to other strictly hyperbolic problems, such as the shallow water equations [21,22], is quite straightforward. This is due to the fact that we have relied principally on the hyperbolic structure of the problem and on the properties of the numerical flux.

Acknowledgements.

The authors wish to thank L. Barbareschi for her valuable contribution and suggestions.

REFERENCES

1. B. Robinson, J. Bathina, and H. Yang, Aeroelastic analysis of wings using the euler equations with a deforming mesh, in *AIAA Structures, structural dynamics and materials conference*, 1990.
2. A. Jameson, W. Schmidt, and E. Turkel, Numerical solution of the euler equations by finite volumes methods using runge-kutta time-stepping schemes, *AIAA*, vol. 81, pp. 1–19, 1981.
3. B. V. Leer, Flux-vector splitting for the euler equations, in *Eighth international conference on numerical methods in fluid dynamics*, 1982.
4. E. Goldlewski and P.-A. Raviart, *Numerical approximation of hyperbolic systems of conservation laws*. Springer, 1996.
5. C. Hirsch, *Numerical computation of internal and external flows*, vol. volume 2, computational methods for inviscid and viscous flows. Wile, 1990.
6. M. Baum, T. Poinsot, and D. Thevenin, Accurate boundary conditions for multicomponent reactive flows, *J. Comput. Phys.*, vol. 116, pp. 247–261, 1994.
7. N. Okong'o and J. Bellan, Consistent boundary conditions for multicomponent real gas mixtures based on characteristic waves, *J. Comput. Phys.*, vol. 176, pp. 330–344, 2002.
8. R. Prosser, Improved boundary conditions for the direct numerical simulation of turbulent subsonic flows. I. inviscid flows, *J. Comput. Phys.*, vol. 207, pp. 736–768, 2005.
9. R. Martineau and R. Berry, Characteristic boundary conditions for the two-step Taylor-Galerkin fem, *Comput. Methods Appl. Mech. Engrg.*,

vol. 195, pp. 742–762, 2006.

10. C. Rowley and T. Colonius, Discretely non reflecting boundary conditions for linear hyperbolic systems, *J. Comput. Phys.*, vol. 157, pp. 500–538, 1999.
11. P. Batten, C. Lambert, and D. Causon, Positively conservative high resolution convection scheme for unstructured elements, *Int. J. Numer. Methods Engrg.*, vol. 39, pp. 1821–1838, 1996.
12. J. LeVeque, *Numerical methods for conservation laws.* Birkhauser, 1992.
13. B. Cockburn, C. Hou, and C. Shu, The Runge-Kutta local projection discontinuous Galerkin finite element method for conservation laws 4: The multidimensional case, *Math. of Comput.*, vol. 36, pp. 545–581, 1990.
14. J. Ghidaglia and F. Pascal, The normal flux method at the boundary for multidimensional finite volume approximations in cfd, *Eur. J. Mech B-Fluid*, vol. 24, pp. 1–17, 2005.
15. G. Jacobs, D. Kopriva, and F. Mashayek, A conservative isothermal wall boundary condition for the compressible Navier-Stokes equations, *SIAM J. Sci. Comput.*, vol. 30, pp. 177–192, 2005.
16. L. Krivodonova and M. Berger, High order accurate implementation of solid wall boundary conditions in curved geometries, *J. Comput. Phys.*, vol. 211, pp. 492–512, 2006.
17. T. Toulorge, Y. Reymen, and W. Desmet, A 2d discontinuous Galerkin method for aeroacustics with curved boundary treatment, in *Proceeding of ISMA*, 2008.
18. A. Rohde, Eigenvalues and eigenvectors of the Euler equations in general geometries, *AIAA*, vol. 1, pp. 2001–2609, 2001. http://www.microcfd.com/download/pdf/AIAA2001-2609.dpf.
19. V. Selmin, The node-centred finite volume approach: bridge between finite differences and finite elements, *Comput. Methods Appl. Mech. Engrg.*, vol. 102, pp. 107–138, 1993.
20. G. F. Franklin, J. D. Powell, and A. Emami-Naeini, *Feedback Control of Dynamic Systems.* Prentice Hall, 2002.
21. D. Givoli, High-order nonreflecting boundary conditions for the dispersive shallow water equations, *J. Comput. Appl. Math.*, vol. 158, pp. 49–60, 2003.
22. A. Holstad and I. Lie, Transparent boundary conditions for the shallow water equations with a mixed finite element formulation, *Appl. Numer. Math.*, vol. 44, pp. 109–138, 2003.